

ECG-Derived Respiration and Instantaneous Frequency based on the Synchrosqueezing Transform: Application to Patients with Atrial Fibrillation

Running Title: EDR and SST-IF in Patients with AF

Yi-Hsin Chan^{1,2¶}, Hau-Tieng Wu^{3¶}, Shu-Shya Hseu⁴, Chi-Tai Kuo^{1,2}, and Yung-Hsin Yeh^{1,2*}

¶These authors contributed equally to this work, ¹First Division of Cardiovascular Department, Chang Gung Memorial Hospital, Linkou, Taoyuan, Taiwan; ²College of Medicine, Chang Gung University, Taoyuan, Taiwan; ³Department of Mathematics, Princeton University, Princeton, NJ 08544, United States; ⁴Department of Anesthesiology, Taipei Veterans General Hospital, Taipei, Taiwan.

* E-mail: yeongshinn@adm.cgmh.org.tw

Reprint requests: Yung-Hsin Yeh, MD, First Division of Cardiovascular Department, Chang Gung Memorial Hospital, Linkou, 5, Fushin street, Kweishan Hsiang, Taoyuan, Taiwan (E-mail: yeongshinn@adm.cgmh.org.tw); Tel: 886-3-3281200, ext 8162; Fax:886-3-3271192

ABSTRACT

The acquisition of information about respiratory patterns without directly recording the respiratory signals would be beneficial in many clinical settings. The electrocardiogram (ECG)-derived respiration (EDR) algorithm, which derives the respiratory pattern by using the information encoded in ECG signals, enables data acquisition in this manner. However, the traditional EDR algorithm cannot be used in patients with atrial fibrillation (AF) because they have highly irregular heart rates. In this paper, we first provide a definition of *ideal instantaneous frequency (IIF)* of respiratory signals and then describe how a novel time–frequency representation technique referred to as the *Synchrosqueezing transform (SST)* was used for the accurate estimation of the *IIF* of respiratory signals, i.e., *SST-IF*. Then, we introduce a new EDR algorithm based on the evaluation of the *SST-IF*. We tested the applicability of our new EDR algorithm in patients with comorbid cardiovascular diseases, most of which were complicated by AF. The study population comprised 16 patients each with sinus rhythm (SR) and persistent AF. The proposed *IIF* was found to match our intuitions, and it was estimated from the ECG signals with the relative median errors as low as 0.32% and 1.12% in the SR group and AF group, respectively. The EDR algorithm exhibited high accuracy in the evaluation of oscillatory respiratory patterns. To the best of our knowledge, this is the first EDR algorithm that can be used in patients with obvious atrial arrhythmias.

Keywords *ECG-derived respiration (EDR); Atrial fibrillation; Instantaneous frequency; Synchrosqueezing transform; Non-uniform sampling; SST-IF*

INTRODUCTION

Abnormal respiratory patterns are observed in several pathological conditions, such as congestive heart failure, central nervous system diseases, chronic lung disease, sleep apnea, metabolic disorders, etc. The precise analysis of abnormal respiratory patterns might facilitate the prediction of the patient's prognosis and the choice of the appropriate treatment [1,2]. Respiratory signals are traditionally recorded by devices such as pressure sensors attached to a strain gauge or a single band wrapped around the chest or abdominal wall, impedance sensors placed over the chest wall, and thermistors placed at the nose. However, there are 2 common disadvantages of using these devices: First, the complex devices involved might interfere with natural physiological breathing. Second, such devices cannot be used for certain clinical purposes, for example, ambulatory or long-term monitoring in naturalistic settings. Therefore, the development of a convenient method to record or estimate respiratory signals is important from a clinical perspective.

ECGs are the most well-known, feasible, and accessible tools in diagnostic medicine. ECGs encode data comprising both electrophysiological cardiac signals and mechanical respiratory signals. The study of respiration-induced distortion of ECG signals started in 1950 [3,4]. Physiologically, there are 2 major causes of the distortion. First, the respiration-related mechanical changes affect the thoracic electrical impedance [5]; the cardiac axis rotation occurring during the respiratory cycle has been shown to be the largest factor contributing to the distortion of the ECG signals [6]. Second, respiration affects the heart rate variability (HRV), thereby causing respiratory sinus arrhythmia [7-10]. Many ECG-derived respiration (EDR) algorithms have been developed to analyze

the respiratory pattern on the basis of the abovementioned physiological factors. These EDR algorithms are essentially classified into 2 major groups according to the applied physiological principles. One group of algorithms is based on analyzing the ECG morphology of the respiratory signals [6,11], while the second group is based on the power-spectrum analysis of HRV [12,13]. Several EDR algorithms have been discussed previously [12,14,15].

Atrial fibrillation (AF) is a serious condition associated with high mortality and morbidity [16]. The rise in the prevalence of AF has paralleled the increase in the life-expectancy of individuals, and AF affects more than 5% of individuals older than 65 years. To the best of our knowledge, traditional EDR techniques are not applicable to AF patients. There are 2 main reasons. First, in methods based on analyzing the QRS complex, cubic-spline interpolation is rendered inaccurate by the high irregularity of the variation in the R-R interval (RRI). Second, the methods based on analyzing the HRV cannot be used because of the well-known white-noise behavior of the HRV in AF patients [17-19]. In the light of the high prevalence of AF patients in clinical practice, it is necessary to develop an EDR algorithm that is suitable for such patients.

In this paper, we first provide a model describing the respiratory signal and a definition of *ideal instantaneous frequency of the respiratory signal (IIF_R)*. Further, we discuss a novel time-frequency analysis technique, namely, *Synchrosqueezing transform (SST)* [20-23]. We then introduce our newly developed EDR algorithm based on estimating *IIF_R* from the ECG signals via *SST*. The newly developed algorithm utilizes the information encoded in the distorted ECG morphology, that is, the varying amplitudes of the R peaks, to achieve the reconstruction. The applicability of the algorithm was

tested not only in healthy subjects but also in AF patients. Moreover, the entire process of the algorithm is rigorously supported by the theories presented in previous studies [22,23].

MODEL, THEORY, AND METHOD

Ethics Statement

Written informed consent was obtained from each participant. The study protocol was approved by the Chang Gung Memorial Hospital Ethics Committee.

Model for the respiratory signal and the notion of instantaneous frequency

We start from modeling the recorded respiratory signal as

$$R(t) = A(t)s(2\pi\phi(t)) + W(t) \quad (1)$$

where for all t , $A(t) > 0$, $|A'(t)| \ll 1$, $\phi'(t) > 0$, $|\phi''| \ll 1$, $s(t)$ is a continuous periodic function defined on $[0, 2\pi]$ with $|\hat{s}(k)| < \delta|\hat{s}(1)|$ for all $k \neq 1$, where δ is positive, and $W(t)$ is the independent noise. $A(t)$ refers to the amplitude modulation function; $s(t)$ refers to the shape function [23]; and $\phi(t)$ refers to the phase function. The shape function under consideration may be different from the Fourier harmonic function, $\cos(t)$. The shape function has been discussed in details previously [23]. The *ideal instantaneous frequency (IIF)* of $R(t)$, denoted by IIF_R , is defined as the derivative of the phase function with respect to t , that is, $\phi'(t)$. The notion of *IIF* is a natural generalization of the notion of the frequency defined by the Fourier transform [22,24]. Several methods have been proposed to estimate IIF_R from $R(t)$ [24]. In this paper, we

focused on the *SST* [21,22], which is described in the next subsection.

The theory of *SST*

SST is a novel adaptive time–frequency analysis technique, which has been presented and analyzed theoretically in previous studies [21-23]; it provides an accurate estimation of *IIF_R*. *SST* involves 3 steps: Given a function $f(t)$ satisfying Equation (1). First, the continuous wavelet transform (CWT) $W_f(a,t)$ of $f(t)$ is calculated [25], with the chosen mother wavelet being ψ , such that $\psi \in C^\infty$, and the support of $\hat{\psi}$ is a subset of $[1-\Delta, 1+\Delta]$ with Δ small enough. Second, the function providing information about *IIF*, $\omega_f(a,t)$, is calculated at each location (a,t) on a subset of (a,t) so that $|W_f(a,t)| > \gamma$, where $\gamma > 0$ is the pre-assigned threshold. Finally, $W_f(a,t)$ is squeezed via re-assignment based on $\omega_f(a,t)$ to obtain the *SST*.

$$S_f^{\alpha,\gamma}(t,\xi) = \int_{A(t)} \frac{1}{\alpha} h\left(\frac{|\omega_f(a,t) - \xi|}{\alpha}\right) W_f(a,t) a^{-3/2} da \quad a \in \mathbb{R}^+ \quad (2)$$

where $A(t) := \{(a,t) : |W_f(a,t)| \geq \gamma\}$, and here, α is the pre-assigned accuracy and

$$h(t) = \frac{1}{2\alpha} \chi_{[-\alpha,\alpha]}.$$

The *SST* algorithm has some properties that render it suitable for use in our EDR algorithm. First, it is easy and convenient to read the information about *IIF* from the $S_f^{\alpha,\gamma}(t,\xi)$ figure. Indeed, only near the $(t, \phi'(t))$ can the value of $|S_f^{\alpha,\gamma}(t,\xi)|$ be “large” [22]. Second, *SST* is an invertible transformation, that is, $f(t)$ can be reconstructed from $S_f^{\alpha,\gamma}$. Indeed, $f(t) = C \int S_f^{\alpha,\gamma}(t,\xi) d\xi$, where C is some universal constant, depending on

the chosen mother wavelet, ψ . Third, *SST* is robust to noise [23], which is the main property of *SST* that makes our EDR algorithm possible. Detailed discussions on and the theoretical proofs of these properties have been provided previously [20-23].

The numerical implementation of the *SST*

The numerical implementation of the *SST* is discussed in this subsection. A more detailed discussion is provided elsewhere [23]. Denote the signal satisfying Equation (1) by $f(t)$ and the digitized respiratory signals, by the vector $\tilde{f} \in R^n$, where $n=2^{L+1}$ and L is a nonnegative integer. Denote the sampling interval by Δt . Thus, $\tilde{f}(m) = f(t_m)$, $m = 1, \dots, n$, where $t_m = m\Delta t$. To prevent boundary effects, we pad \tilde{f} on both sides using reflecting boundary conditions.

The CWT is implemented by sampling the continuous wavelet transform, W_f , at the locations (a_j, t_m) , where $a_j = 2^{j/n_v} \Delta t$, $j = 1, \dots, L_{n_v}$, and the number of voices, n_v is a user-defined “voice number” parameter. We save the result as the $L_{n_v} \times n$ matrix $\tilde{W}_{\tilde{f}}$.

The function providing the *IIF* information, ω_f , is implemented as an $L_{n_v} \times n$ matrix and is denoted by $\tilde{\omega}_{\tilde{f}}$. Fix the threshold as $\gamma > 0$, and $\partial_b W_f(a, b)$ is implemented by the finite difference with respect to b and is denoted by $D_b \tilde{W}_{\tilde{f}}$. For each $j = 1, \dots, L_{n_v}$ and $m = 1, \dots, n$, when $\tilde{W}_{\tilde{f}}(j, m) > \gamma$, evaluate

$$\tilde{\omega}_{\tilde{f}}(j, m) = -\frac{i}{2\pi} D_b \tilde{W}_{\tilde{f}}(j, m) \tilde{W}_{\tilde{f}}(j, m)^{-1} \quad (3)$$

otherwise, set $\tilde{\omega}_{\tilde{f}}(j, m)$ to be infinity.

To implement $S_f^{\alpha,\gamma}(t, \xi)$, we first discretize the frequency domain, ξ , as follows.

First, choose the frequency interval of interest, say, $[\bar{\xi}, \underline{\xi}]$. The valid $\bar{\xi}$ is limited by the

Nyquist theorem, that is, $\bar{\xi} \leq \frac{1}{2\Delta t}$. The valid $\underline{\xi}$ is limited by the maximum period of the

input signal, that is, $\underline{\xi} \geq \frac{1}{n\Delta t}$. We assume $\bar{\xi} = \frac{1}{2\Delta t}$ and $\underline{\xi} = \frac{1}{n\Delta t}$. We discretize $[\bar{\xi}, \underline{\xi}]$ by

$\xi_l = 2^{(l-1)\Delta\omega} \underline{\xi}$, $l = 1, \dots, n_\xi$, with $\Delta\xi = \frac{1}{n_\xi - 1} \log_2(n/2)$, where n_ξ is the user-defined

parameter, which determines the resolution of the *IIF* estimation. Denote

$$B_{l,m} := \left\{ j : \left| \tilde{W}_f(j, m) \right| > \gamma; \text{ROUND} \left[\frac{1}{\Delta\xi} \log_2 \left(\frac{\tilde{\omega}_f(j, m)}{\xi_l} \right) \right] \right\}$$

where *ROUND* is rounding to integer. Denote the implemented $S_f^{\alpha,\gamma}(t, \xi)$ by \tilde{S}_f^γ , which

is

$$\tilde{S}_f^\gamma(m, l) = \sum_{j \in B_{l,m}} \frac{\log 2}{n_\nu} \tilde{W}_f(j, m) a_j^{-1/2} \quad (4)$$

where $l = 1, \dots, n_\xi$, $m = 1, \dots, n$. According to the property of the *SST* proved in Theorem

3.3 in the paper by Daubechies *et al* [22] and Theorem 2.5.4 in Wu [23], the value of $\left| \tilde{S}_f^\gamma \right|$

is large only near the $(t_m, \phi'(t_m))$, and the discretized curve, a vector $c^* \in Z_{n_\xi}^n$, where

$Z_{n_\xi} = \{1, 2, \dots, n_\xi\}$, fitting the dominant area of \tilde{S}_f^γ represents the *IIF* of $f(t)$ with high

accuracy. The dominant area is fit by the curve c^* by maximizing the following

functional:

$$\max_{c \in (\mathbb{Z}_{n_{\xi}})^n} \left[\sum_{m=1}^n \log(q^{-1} |\tilde{S}_f^{\gamma}(c(m), m)|) - \lambda \sum_{m=2}^n |c(m) - c(m-1)|^2 \right] \quad (5)$$

where $q = \sum_{m,l} |\tilde{S}_f^{\gamma}(l, m)|$ is a normalizing constant. The user-defined parameter $\lambda > 0$ determines the “smoothness” of the resulting curve estimate. For the sake of convenience, we shall use the acronym for the *SynchroSqueezing Transform-derived Instantaneous Frequency* and the vector $SST-IF_f = 2^{(c^*(m)-1)\Delta\omega} \underline{\xi}$ of $f(t)$ to represent the estimated *IIF* in the following discussion.

According to Theorem 2.5.4 in Wu [23], the signal f can be reconstructed accurately by

$$\tilde{f}(m) = \sum_{l \in N_m} \tilde{S}_f^{\gamma}(l, m) \quad (6)$$

where $m = 1, \dots, n$, $N_m = \{c^*(m) - n_w, c^*(m) - n_w + 1, \dots, c^*(m) + n_w - 1, c^*(m) + n_w\}$ and n_w is the user-defined parameter.

The *IIF* estimation of the respiratory signal

When we evaluate *SST-IF_R* from the respiratory signal, we employ the following parameters: we choose the mother wavelet, ψ , such that it satisfies $\hat{\psi}(\xi) = 2^{-((\xi-1)/0.15)^2}$ (To be a “true wavelet,” ψ should satisfy $\hat{\psi}(0) = 0$, which is not strictly the case here, but it is true for all practical purposes), $n_v = 32$, and $\gamma = 10^{-8}$; the parameter for the curve extraction is $\lambda = 5$. Note that *SST-IF_R*(m) is the estimation of *IIF_R* at time t_m . In the section “**Validity of the *SST-IF* defined via the *SST***”, we demonstrate that *SST-IF_R* echoes the intuitive concept of instantaneous frequency of the respiratory signal.

The new EDR algorithm based on *SST*

The EDR algorithm consists of 3 steps: (1) pre-processing for removing the baseline wandering, (2) construction of the traditional EDR according to the detection of R-peaks and cubic spline interpolation, and (3) estimation of IIF_R from the traditional EDR and reconstruction of the respiratory signal via the SST . The lead II ECG signal, $ECG_{II}(t)$, is digitalized at time $t_m = m\Delta t$, where $m = 1, \dots, N$ and Δt is the sampling interval. The processing steps applied to the given ECG signal are detailed below:

Step 1: We apply the median filter to remove the baseline wandering: we choose the moving window of length $ROUND(\frac{1}{10\Delta t})$, which is chosen such that it is longer than the average length of the QRS complex.

Step 2: We construct the traditional EDR signal from the lead II ECG signal. If the cardiac axis is within the normal range of $-30-90^\circ$ with the Rs pattern shown in the lead II ECG, we detect the timing of the R peaks; otherwise, we detect the timing of the S peaks with the condition of the rS pattern. We exclude all the existing PVC beats. Suppose that there are N_R R-peaks (or S-peaks when the cardiac axis is deviated) in the recorded lead II ECG signal and their timing is t_i , where $i = 1, \dots, N_R$. The traditional EDR signal, denoted as EDR_T , is obtained by the cubic spline interpolation on the data points $\{t_i, ECG_{II}(t_i)\}$ [6].

Step 3: We run the SST on $EDR_T(t)$ and get the time-frequency representation $\tilde{S}_{EDR_T}^\gamma$. We estimate the IIF_R by Equation (5). The result is denoted by the vector $SST-IF_E$, where $SST-IF_E(m)$ is the estimation of IIF_R at time t_m . The respiratory signal is reconstructed by Equation (6). The result is our EDR signal.

When we run our EDR algorithm, we employ the following parameters in the SST: we choose the mother wavelet, ψ , which satisfies $\hat{\psi}(\xi) = 2^{-((\xi-1)/0.125)^2}$, $n_v = 32$, and $\gamma = 10^{-8}$; the parameter for the curve extraction is $\lambda = 10$, and the parameter for the respiratory signal reconstruction is $n_w = 80$.

Subjects, data acquisition, and processing

We enrolled 58 individuals (26 patients with sinus rhythm (SR) and 32 patients with persistent AF) in our study. All patients underwent echocardiography (ViVid 7, General Electric Vingmed Ultrasound, Horten, Norway) to evaluate the systolic heart function or to detect any structural heart disease. Of the 58 patients, 26 were excluded from the analysis on the basis of the following criteria: (1) the ratio of the number of premature ventricular complex (PVC) beats to the number of total beats (TB) was $>4\%$; (2) the patients had Cheyne-Stokes respiration (CSR) or other irregular respiratory patterns, which were clinically verified by well-trained physicians; and (3) patients had impaired left ventricular systolic ejection fraction (EF) ($EF < 55\%$), as determined by M-mode echocardiography. The final study population comprised 16 patients each with SR and persistent AF. During the experiment, each patient was allowed to breathe freely without any restrictions of respiration frequency or intensity. Most patients were awake during the entire measurement period. The ECG and mechanical respiratory signals were recorded simultaneously for about 20 minutes after the patients lay in the supine position for more than 10 minutes. Lead II ECG signal was obtained for 20 minutes (1200 seconds) with a commercial Holter machine (My ECG E3-80, MSI, Inc., Taiwan). The ECG sampling rate was 1000 Hz, and the resolution was 12 bits. To ensure proper identification of abnormal P waves or QRS complexes, the ECG recordings of all the patients were

visually reviewed to confirm the presence of SR; persistent AF; or other arrhythmias, such as PVC and premature atrial complex (PAC). R/S peaks were detected using the MSI HRV software (MSI, Inc., Taiwan). Time-domain HRV measurements (Table 1), including mean RR interval, RMSSD, SDNN, TINN, NN50, and PNN50, were calculated for the entire length of the ECG obtained for each patient. The clinical characteristics, cardiovascular disease diagnosed on the basis of two-dimensional (2D) echocardiography or past medical history, and EF and HRV profiles of the patients have been listed in Table 2. A pneumatic respiration belt (CI-6535, PASCO, Inc., California, USA) was wrapped around the chest of the patient to measure the thoracic wall movement during the respiration, and the obtained measurements were used as the true respiratory signal for reference. The analog respiratory signal was converted to a digital signal via an A/D converter, which was finally recorded and processed by the ScienceWorkshop 750 system (PASCO, Inc., California, USA). The sampling rate was 20 Hz, and the resolution was 8 bits. After the measurement, the recorded ECG and respiratory signals were processed using the Matlab software (The Mathworks, Natick, MA, USA) for further analysis.

Comparison between $SST-IF_R$ and $SST-IF_E$

To evaluate the accuracy of estimating IIF_R from the lead II ECG, i.e., the vector $SST-IF_E$, we determine the relative percentage error compared to $SST-IF_R$, the estimated IIF_R from the respiratory signal, in the following manner. Divide the total record time period, $[0, T]$, into K sequential non-overlapping segments I_i , $i=1, \dots, K$, where each I_i is of

length T/K seconds. Evaluate $SST-IF_{R,i} = \frac{1}{|I_i|} \sum_{t_j \in I_i} SST-IF_R(j)$ and

$SST-IF_{E,i} = \frac{1}{|I_i|} \sum_{t_j \in I_i} SST-IF_E(j)$, $SST-IF_{R,i}$ (resp. $SST-IF_{E,i}$) stands for the averaged $SST-IF_R$

(resp. $SST-IF_E$) over the time segment I_i . Next, evaluate

$\delta_i = \frac{SST-IF_{R,i} - SST-IF_{E,i}}{SST-IF_{R,i}} \times 100\%$, which is the relative percentage error of the estimation

over the time segment I_i . The performance of the overall estimation E_K is represented by

$$E_K = median_i \delta_i \quad (7)$$

where the median is used in order to reduce the influence of a few outlier values. In this study, T is fixed at 20 minutes, and we consider 3 different K , namely, $K = 240$, $K = 120$, and $K = 20$ ($T/K = 5$, 10, and 60 seconds, respectively).

RESULTS

Validity of the $SST-IF$ defined via the SST

We show that $SST-IF_R$ echoes the intuitive concept of instantaneous frequency of the respiratory signal. First, we intuitively define the notion of time-dependent instantaneous respiration rate as the inverse of the time interval between the 2 most recent successive breathing cycles. A breathing cycle is defined as the signal between 2 consecutive ends of inspiration. In particular, denote the end of the inspiration in the recorded respiratory signal by t_i , $i=1, \dots, M$. The intuitive instantaneous respiration rate, denoted as $IRR_i(t)$, where the subscript i refers to the ‘‘intuitive’’ character of this definition, is defined as a piecewise constant function:

$$IRR_i(t) = 1 / (t_k - t_{k-1}) \text{ when } t_k \leq t < t_{k+1} \quad (8)$$

This definition echoes the notion of frequency: counting how frequently waves appear in a unit time period. The IRR_i is demonstrated as the black piecewise-constant curve in Figure 1.

Next, we demonstrate that the $SST-IF_R$ captures IRR_i . The result of $SST-IF_R$ is shown as the red dash curve in Figure 1. We can see that $SST-IF_R$ matches IRR_i closely. This result justifies the introduction of $SST-IF_R$ to numerically represent the intuitive instantaneous frequency. Since $SST-IF_R$ is an accurate estimation of IIF_R , we conclude that the IIF notion defined in the model is meaningful in the sense of capturing our intuition.

The IIF estimation of the respiratory signal

Table 2 summarizes the patients' clinical characteristics, diagnosis, HRV profiles, and EF. No significant difference was found between the SR and AF groups in terms of patient age (average \pm 1 SD: 66.19 ± 14.49 years vs. 71.38 ± 11.21 years), EF ($68.88 \pm 7.21\%$ vs. $71.75 \pm 8.23\%$), PVC number (0.94 ± 3.75 vs. 5.94 ± 13.15), TB number (1474.38 ± 182.92 vs. 1376.31 ± 236.90), PVC/TB ratio ($0.06 \pm 0.23\%$ vs. $0.45 \pm 0.99\%$), and mean R-R interval (829.00 ± 90.66 ms vs. 900.19 ± 160.41 ms). The SR and AF groups showed significant difference in the HRV profile, including RMSSD (25.13 ± 20.61 ms vs. 256.81 ± 75.26 ms), SDNN (28.25 ± 16.40 ms vs. 179.13 ± 52.43 ms), TINN (103.56 ± 49.77 ms vs. 474.88 ± 236.07 ms), NN50 (35.75 ± 57.24 vs. 762.81 ± 211.91), and PNN50 ($2.70 \pm 4.48\%$ vs. $76.16 \pm 9.80\%$). Table 3 summarizes the gross median error of $SST-IF_E$ in the segments of 5, 10, and 60 seconds (E_5 , E_{10} , and E_{60}) for each patient. The results indicated that $SST-IF_R$ agreed well with $SST-IF_E$, for all participants, irrespective of whether they had SR or AF. The SR group showed slightly

better accuracy than the AF group in the segments of 5 ($0.90 \pm 0.48\%$ vs. $1.97 \pm 0.76\%$), 10 ($0.78 \pm 0.44\%$ vs. $1.69 \pm 0.68\%$), and 60 ($0.32 \pm 0.22\%$ vs. $1.12 \pm 1.01\%$) seconds. We illustrate the *IIF* estimation results, that is, $SST-IF_R$ and $SST-IF_E$, of a SR patient (*Patient G*) and an AF patient (*Patient i*) in Figures 2 and 3, respectively.

The estimation of the respiratory signal—the EDR from our new algorithm

In Figures 4 and 5, we present the results of applying our EDR algorithm to one subject each with SR (*Patient B*) and AF (*Patient l*). In both figures, the reference signal, the EDR signals based on the traditional algorithm, and the EDR signal derived using our new algorithm are denoted by *red, black, and blue curves*, respectively. The results presented in Figure 4 (*Patient B*) indicate that our EDR signal matches well with the reference respiratory signal, while the amplitude does not. Notably, our EDR signal successfully recognized 3 hypoapnea beats (denoted by the *black arrow*) among the total 118 beats in the reference signal. Figure 5 (*Patient l*) also shows that our EDR signal had good correlation with the reference signal for the AF patient.

Patients with abnormal periodic respiration pattern

Subjects with the CSR pattern were excluded from the study group. However, we found that our new EDR algorithm was useful in some of these excluded patients. We present the obtained results. The 4 excluded subjects showed a cyclic respiration pattern characterized by alternating apnea and hyperpnea with a crescendo-decrescendo pattern, during the entire measurement period. Each cycle lasted for around 50 to 100 seconds. Table 4 summarizes the clinical characteristics, diagnosis, HRV profiles, and EF of these patients. Note that 3 (*Patient Q*, *Patient r*, and *Patient s*) of the 4 patients had poor EF ($EF < 55\%$). The EDR signal could be reconstructed successfully in *Patient Q*, *Patient q*,

and *Patient s*, while it failed in *Patient r*. Figures 6 and 7 illustrate the *IIF* estimation and the EDR signal for *Patient q*. Figure 7 shows that the hyperpnea and apnea phases of the reference signal (*red curve*) lasted for ~30 seconds and ~20 seconds, respectively. Note that our EDR signal (*blue curve*) matches well with the oscillatory respiration pattern derived from the reference signal (*red curve*), in both the apnea and hyperpnea phases. The E_5 , E_{10} , and E_{60} of $SST-IF_E$ in these patients are summarized in Table 5. Note that the gross median errors in *IIF* estimation for *Patient Q*, *Patient q*, and *Patient s* are larger than those for patients without CSR (Table 3).

DISCUSSION

We propose a new EDR algorithm based on the notion of *IIF* and the novel adaptive time–frequency analysis technique, *SST*. First, we build up a traditional EDR signal $EDR_T(t)$ from the amplitudes of the R peaks of the ECG signal. Then, $EDR_T(t)$ is analyzed by the *SST* to estimate the *IIF* and reconstruct the respiratory signals. We tested the applicability of our method to AF patients with multiple comorbid cardiovascular diseases (Table 2). We found that the estimated respiratory signals reflected the oscillatory pattern of the reference respiratory signals simultaneously recorded from the chest-belt respiration sensor. In particular, the estimated *IIF* of the respiratory signals derived from the ECG lead II exhibited minimal error for both SR and AF patients ($E_{60} = 0.32\%$ and $E_{60} = 1.12\%$, respectively). Thus, besides being useful in AF patients, our EDR algorithm may have wider medical applications since it requires the recording of only lead II ECG signal.

The exclusion criteria defined in this study merit some discussion. First, our algorithm cannot be applied to subjects with irregular respiration patterns because Equation (1) would not be satisfied in this case. However, when irregular respiration has a fixed pattern, for example, CSR with a crescendo-decrescendo pattern, our new EDR algorithm may be helpful. Second, even if the patients have regular respiration patterns, no EDR algorithm can guarantee any success when the number of PVC beats is high. The morphology of PVC is extremely bizarre. Further, these beats are often random and are followed by subsequent, resetting normal QRS beats. These properties render PVC unsuitable for EDR cubic spline interpolation or HRV spectral analysis. Therefore, subjects with $PVC/TB > 4\%$ were excluded from this study. However, since the prevalence of PVC episodes in patients with advanced cardiovascular diseases is high, further studies are necessary for the development of an improved EDR algorithm that would be applicable to these patient groups.

Frequent PAC was not considered as an exclusion criterion in our study. Although the P-wave morphology of PAC is markedly different from that of the SR beat, the QRS morphology in both types of beats are similar because the AV conduction pathway is common in both cases. Thus, the R peaks of the PACs can be considered as informative as those of the normal beats. This supposition is confirmed by the results obtained for **Patient d** (Figure 8). In this patient's ECG, the P wave could be recognized before each QRS beat (not shown here). However, the RR interval was irregular due to frequent PACs (PAC number/TB number: 210/1372), which make its HRV profile similar to the AF pattern. We estimated the *IIF* with PAC preservation and removal. The results (Figure 8) showed that PAC preservation afforded a higher accuracy in *IIF* estimation than PAC

removal, indicating that the R peaks of the PAC beats were also informative to the EDR algorithm.

Next, we discuss how the EDR algorithm performed in several interesting cases included in this study. **Patient E** had complete AV block and had undergone implantation of a permanent pacemaker with the DDDR mode. The sensed AV delay was set at 150 ms. Satisfactory *IIF* estimation and EDR signal were obtained for this patient (Table 3), indicating that our EDR algorithm has potential to be applied in patients with artificial cardiac pacing. Further, 2 patients in this study had a wide QRS complex with left bundle branch block (LBBB) (**Patient j**) and right bundle branch block (RBBB) (**Patient J**). The results revealed that consistent wide-QRS complexes did not interfere with the accuracy of our EDR algorithm. One patient had an episode of supraventricular tachycardia (SVT) during data acquisition (**Patient K**). At the beginning of data acquisition, **Patient K** was in SR, with a basic cycle length (BCL) of 760 ms. Since the 1004th second, the patient experienced sustained SVT triggered by an ectopic PAC, with a BCL of 440 ms. The respiration frequency increased during the SVT attack (Figure 9 A). The estimation of *IIF* and the EDR signal both in the SR and SVT phases were satisfactory. Compared to the EDR signal obtained by the traditional algorithm, which is distorted, our EDR algorithm provides better EDR signal during the SVT attack (Figure 9 B).

Although subjects with sleep apnea and those with the CSR pattern were excluded from the study group, as discussed earlier, our new EDR algorithm may be useful to some extent on these subjects. Sleep apnea is a common sleep disorder with high prevalence in adults [26]. Traditionally, the diagnosis of sleep apnea relies on the complicated and expensive process of polysomnography performed overnight in sleep laboratories.

Several recent studies have been conducted to test the feasibility of EDR algorithms as an alternative tool for sleep apnea detection because it facilitates the recording of both cardiac and respiratory signals with minimal interference, comfort to the patient, and reliable signal processing/acquisition [27-31]. The design of our experimental algorithm was not specific for the identification of sleep apnea—our measurement time was limited to 20 minutes, and most patients were awake during the experiment. However, a few patients did fall asleep during the measurements, and one of them had AF (*Patient q*). This AF patient showed a cyclic respiratory pause (each pause lasted around 20 seconds) within 20 minutes of the measurement time, which is partially compatible with the diagnostic criteria of sleep apnea (A patient with more than 5 apnea events, where each event is defined as a respiratory pause of more than 10 seconds, per hour during a full night's sleep is diagnosed with sleep apnea according to the AASM criteria [26]). Although the *IIF* estimation was not as good as that obtained for patients with a regular respiration pattern ($E_{60} = 3.61\%$; Figure 6), as shown in Figure 7, the EDR signal matched well with the oscillatory respiration pattern. The CSR pattern, which is recognized in patients with advanced heart failure (HF), ultimately contributes to high risk of mortality in the future [1]. In our study, 3 patients with poor left ventricular systolic function were awake during the ECG recording: one had SR (*Patient Q*) and the others had AF (*Patient r* and *Patient s*). All 3 patients showed the waxing and waning breathing pattern during the measurement time. Our EDR algorithm provided a satisfactory EDR signal for the HF patient with SR (*Patient Q*). However, for the one subject with both HF and AF (*Patient r*), we could not get convincing results. Thus, since our EDR algorithm is capable of recovering the oscillation pattern of the respiratory

signal in some of the patients with sleep apnea or the CSR pattern, a more large-scale study using our EDR algorithm is warranted with dedicated overnight sleep monitoring or intensive care unit monitoring.

The stability of the *SST* [20,23] plays a major role in our EDR algorithm. In fact, with the error estimate on cubic spline approximations [32],

$$\|R - EDR_T\|_{L^\infty} \leq \frac{5}{384} D^4 \|R^{(4)}\|_{L^\infty} \quad (9)$$

where $\|\cdot\|_{L^\infty}$ is the uniform bound, D is the maximal RR interval, R is the true respiratory signal, $R^{(4)}$ is the fourth derivative of R , and EDR_T is the traditional EDR derived from the cubic spline, the error in *IIF* estimation can be determined by the stability theorem 2.3.17 in Wu [23]. Therefore, in AF patients, the more irregular the RR intervals, the greater are the 4th order derivatives of the respiratory signal and the poorer is the estimation. By the same argument, in the patients with PVC, since the EDR_T is compromised because PVC beats are removed, it can be inferred that the more random the PVCs, the poorer the estimation is.

We believe that if more leads are available, then by the technique proposed in previous studies [6,11] evaluating the cardiac rotation, the final EDR result can be improved by obtaining a better EDR_T . In addition, taking HRV into consideration might be useful for young and active subjects who are free of arrhythmia. Furthermore, evidence clearly shows that information about some characteristics of the respiratory signal, such as the shape function of respiration, is inevitably lost by the ECG signal. In other words, our new EDR algorithm, similar to other EDR algorithms, cannot fully recover the respiratory signal. In particular, the shape function of the respiratory signal

defined in Equation (1) can not be recovered.

In conclusion, we present a novel method for monitoring respiration in clinical practice. To the best of our knowledge, this is the first EDR algorithm applicable to patients with AF or other atrial arrhythmias. Since only a single lead II ECG signal is necessary for our EDR algorithm, we believe that it has potential for wide clinical application.

ACKNOWLEDGEMENT

H.-T. Wu acknowledges support by FHWA grant DTFH61-08-C-00028 and the valuable discussion from Professor Ingrid Daubechies and Professor Chung-Kang Peng.

REFERENCES

1. Somers VK, White DP, Amin R, Abraham WT, Costa F et al. (2008) Sleep apnea and cardiovascular disease. *Circulation* 118: 1080-1111.
2. Wang H, Parker JD, Newton GE, Floras JS, Mak S et al. (2007) Influence of obstructive sleep apnea on mortality in patients with heart failure. *J. Am. Coll. Cardiol.* 49: 1625-1631.
3. Einthoven W, Fahr G, Waart A (1950) On the direction and manifest size of the variations of potential in the human heart and on the influence of the position of the heart on the form of the electrocardiogram. *Am. Heart J.* 40: 163-211.

4. Flaherty J (1967) Influence of respiration on recording cardiac potentials. *Am. J. Cardiol.* 20: 21–28.
5. Houtveen JH, Groot PF, de Geus EJ (2006) Validation of the thoracic impedance derived respiratory signal using multilevel analysis. *Int J Psychophysiol.* 59: 97-106.
6. Moody GB, Mark RG, Zoccola A, Mantero S (1985) Derivation of respiratory signals from multi-lead ECGs. *Computers in Cardiology* 12: 113-116.
7. Berntson GG, Bigger JTJ, Eckberg DL, Grossman P, Kaufmann PG et al. (1997) Heart rate variability: origins, methods, and interpretive caveats. *Psychophysiology* 34: 623-648.
8. Jamsek J, Stefanovska A, McClintock VEP (2004) Nonlinear cardio- respiratory interactions revealed by time-phase bispectral analysis. *Phys. Med. Biol.* 49: 4407–4425.
9. Grossman P, Wilhelm FH, Spoerle M (2004) Respiratory sinus arrhythmia, cardiac vagal control and daily activity. *Am. J. Physiol. Heart Circ. Physiol.* 287: 728–734.
10. Humeau A, Buard B, Mahé G, Chapeau-Blondeau F, Rousseau D et al. (2010) Multifractal analysis of heart rate variability and laser doppler flowmetry fluctuations: comparison of results from different numerical methods. *Phys. Med. Biol.* 55: 6279–6297.
11. Leanderson S, Laguna P (2003) Estimation of the respiratory frequency using spatial information in the VCG. *Medical engineering & physics* 25: 501-507.
12. Cysarz D, Zerm R, Bettermann H, Frühwirth M, Moser M et al. (2008) Comparison of respiratory rates derived from heart rate variability, ECG amplitude, and nasal/oral airflow *Ann Biomed Eng.* 36: 2085-2094.

13. Meste O, Blain G, Bermon S (2002) Analysis of the respiratory and cardiac systems coupling in pyramidal exercise using a time-varying model. *Computers in Cardiology* 22: 429 – 432.
14. Bianchi AM, Pinna GD, Croce M, La Rovere MT, Maestri R et al. (2003) Estimation of the respiratory activity from orthogonal ECG leads. *Computers in Cardiology* 30: 85–88.
15. Clifford GD, Azuaje F, McSharry PE (2006) Advanced methods and tools for ECG data analysis. Artech House. pp. 215-243.
16. Jahangir A, Lee V, Friedman PA, Trusty JM, Hodge DO et al. (2007) Long-term progression and outcomes with aging in patients with lone atrial fibrillation: a 30-year follow-up study. *Circulation* 115: 3050–3056.
17. Costa M, Goldberger AL, Peng CK (2002) Multiscale entropy analysis of complex physiologic time series. *Phys. Rev. Lett.* 89: 0681021-0681024.
18. Friedman HS (2004) Heart rate variability in atrial fibrillation related to left atrial size. *Am. J. Cardiol.* 93: 705–709.
19. Peng CK, Mietus J, Hausdorff JM, Havlin S, Stanley HE et al. (1993) Long-range anticorrelations and non-gaussian behavior of the heartbeat. *Phys. Rev. Lett.* 70: 1343–1346.
20. Thakur G, Wu HT (2010) Synchrosqueezing-based recovery of instantaneous frequency from nonuniform samples. *SIAM J. Math. Anal.* In press. (<http://arxiv.org/abs/1006.2533>)
21. Daubechies I, Maes S (1996) A nonlinear squeezing of the continuous wavelet transform based on auditory nerve models. *Wavelets in Medicine and Biology* CRC-Press. pp. 527-546.

22. Daubechies I, Lu J, Wu HT (2010) Synchrosqueezed wavelet transforms: An empirical mode decomposition-like tool. *Applied and Computational Harmonic Analysis* 30: 243-261.
23. Wu HT (2011) Adaptive analysis of complex data sets. Ph.D. Thesis. Princeton University: U.S.A. pp. 4-71.
24. Flandrin P (1999) Time-frequency/time-scale analysis, wavelet analysis and its applications, vol. 10. Academic Press Inc. pp. 49-301.
25. Daubechies I (1992) Ten Lectures on Wavelets. Society for Industrial and Applied Mathematics Philadelphia, PA, USA. pp. 17-52.
26. Parati G, Lombardi C, Narkiewicz K (2007) Sleep apnea: epidemiology, pathophysiology, and relation to cardiovascular risk. *Am J Physiol Regulatory Integrative Comp Physiol.* 293: 1671-1683.
27. de Chazal P, Heneghan C, Sheridan E, Reilly R, Nolan P et al. (2003) Automated processing of the single-lead electrocardiogram for the detection of obstructive sleep apnoea. *Biomedical Engineering, IEEE Transactions on.* 50: 686 –696.
28. Khandoker AH, Palaniswami M (2011) Modeling respiratory movement signals during central and obstructive sleep apnea events using electrocardiogram. *Ann Biomed Eng.* 39: 801-811.
29. Penzel T, McNames J, Murray A, de Chazal P, Moody GB et al. (2002) Systematic comparison of different algorithms for apnoea detection based on electrocardiogram recordings. *Med. Biol. Eng. Comput.* 40: 402–407.
30. Thomas RJ, Mietus JE, Peng CK, Gilmartin G, Daly RW et al. (2007) Differentiating obstructive from central and complex sleep apnea using an automated

electrocardiogram-based method. Sleep 30: 1756–1769.

31. Thomas RJ, Weiss MD, Mietus JE, Peng CK, Goldberger AL et al. (2009) Prevalent hypertension and stroke in the sleep heart health study: Association with an ECG-derived spectrographic marker of cardiopulmonary coupling. Sleep 32: 897–904.

32. Burden R, Faires J (1993) Numerical Analysis. PWS. 142 p.

FIGURE LEGENDS

Figure 1. The validation of $SST-IF_R$.

The *blue curve* is the recorded respiratory signal, and the *red circle* denotes the end of each inspiration. The intuitive instantaneous respiration rate IRR_i is demonstrated as the *black piecewise constant curve*. The result of $SST-IF_R$ is shown as the *red dash curve*. Note that $SST-IF_R$ matches IRR_i accurately, and hence, the representation of the intuitive notion of instantaneous frequency by $SST-IF_R$ is validated.

Figure 2. The $SST-IF$ for a SR patient (*Patient G*).

The *blue curve* is the $SST-IF_E$ from lead II ECG, and the *red curve* is the $SST-IF_R$. Note that the $SST-IF_E$ approximates $SST-IF_R$ with high accuracy ($E_{60} = 0.21\%$) for the entire measurement period (1200 seconds).

Figure 3. The $SST-IF$ for an AF patient (*Patient i*).

The *blue curve* is the $SST-IF_E$ from lead II ECG, and the *red curve* is the $SST-IF_R$. Note that the $SST-IF_E$ approximates $SST-IF_R$ with high accuracy ($E_{60} = 0.15\%$) during the entire measurement period (1200 seconds).

Figure 4. The result of our EDR signal for a SR patient (*Patient B*).

The reference respiration signal, the traditional EDR signal, and our new EDR signal are denoted by the *red*, *black*, and *blue curves*, respectively. The results indicate that our EDR signal corresponded well with the oscillatory pattern of the reference respiration signal. Note that unlike the traditional signal, our new EDR signal successfully recognized 3 hypoapnea beats (denoted by the *black arrow*) among the 118 beats in the reference signal.

Figure 5. The result of our EDR signal for an AF patient (*Patient l*).

The reference respiration signal, the traditional EDR signal, and our new EDR signal are denoted by the *red*, *black* and *blue curves*, respectively. The results indicate that our EDR signal matched well with the oscillatory pattern of the reference respiration signal.

Figure 6. The *SST-IF* for an AF patient (*Patient q*) with abnormal periodic respiration pattern.

Note that the relative error between the *SST-IF_E* (*blue curve*) and *SST-IF_R* (*red curve*) for this patient is larger ($E_{\delta 0} = 3.61\%$) than those for patients with the normal respiration pattern (Figures 2 and 3).

Figure 7. Our EDR signal for an AF patient (*Patient q*) with an abnormal periodic respiration pattern.

The reference respiration signal, the traditional EDR signal, and our new EDR signal

were denoted by the *red*, *black*, and *blue curves*, respectively. The hyperpnea and apnea phases (denoted by the *black arrow*) of the reference signal alternated with each other and were ~30 seconds and ~20 seconds in duration, respectively. It was noted that our EDR signal matches well with the reference signal both in the apnea and hyperpnea phases.

Figure 8. The SST-IF for an AF patient (*Patient d*) with frequent PAC beats.

The upper subplot **A** is the result of our EDR algorithm when the traditional EDR, EDR_T , is constructed only from the R peaks of normal beats; the *blue curve* is $SST-IF_E$ and the *red curve* is $SST-IF_R$. The lower subplot **B** is the result of our EDR algorithm when EDR_T is constructed from the R peaks of both PAC beats and normal beats; the *blue curve* is $SST-IF_E$ and the *red curve* is $SST-IF_R$. It confirms that the PAC beats are informative to our EDR algorithm.

Figure 9. The STT-IF and EDR signal for a SR patient (*Patient K*).

In subplot A, The *blue curve* is the $SST-IF_E$ and the *red curve* is the $SST-IF_R$; in subplot B, the *blue curve* is the signal obtained using our EDR algorithm, the *black curve* is the signal obtained using the traditional EDR algorithm, and the *red curve* is the reference signal. *Patient K* develops sustained supraventricular tachycardia (SVT) since the 1004th second. Note that the respiration frequency increases during the SVT attack. Compared to the traditional EDR, our EDR algorithm provides better information on the oscillatory respiration pattern during the SVT attack.

Table 1. Heart rate variability (HRV) measurements: abbreviations and definitions

PVC	Number of premature ventricular complex over 20 minutes
TB	Number of total heart beat over 20 minutes
Mean	Mean RR interval over 20 minutes
RMSSD	Root-mean-square of the successive differences of normal RR intervals over 20 minutes
SDNN	SD of all normal RR intervals over 20 minutes
TINN	The triangular interpolation of RR interval histogram over 20 minutes
NN50	Number of successive normal RR intervals that differ by >50 ms over 20 minutes
PNN50	Percentage of successive normal RR intervals that differ by >50 ms over 20 minutes

Table 2. Clinical characteristics, HRV profiles, and cardiac systolic function of the patients

SR	Diagnosis	Age	Sex	PVC	TB	PVC/TB	Mean	RMSSD	SDNN	TINN	NN50	PNN50	EF
<i>A</i>	VHD/PH	80	F	0	1408	0.00%	852	44	37	109	48	3.46%	68%
<i>B</i>	VHD/PH	78	F	0	1391	0.00%	862	25	20	78	19	1.39%	66%
<i>C</i>	VHD/LVH	82	F	15	1611	0.93%	745	36	32	78	48	3.17%	78%
<i>D</i>	LVH	70	F	0	1757	0.00%	682	8	19	94	0	0.00%	68%
<i>E</i>	PPM	82	F	0	1286	0.00%	932	11	13	78	0	0.00%	71%
<i>F</i>	IHD	59	M	0	1238	0.00%	968	69	58	188	4	0.32%	63%
<i>G</i>	LVH	80	F	0	1373	0.00%	873	26	32	125	47	3.55%	68%
<i>H</i>	LVH/CVA	54	M	0	1336	0.00%	898	7	8	47	0	0.00%	80%
<i>I</i>	LVH/IHD	60	M	0	1424	0.00%	842	27	37	156	50	3.52%	66%
<i>J</i>	LVH/RBBB	71	F	0	1443	0.00%	831	13	17	78	3	0.21%	65%
<i>K</i>	VHD/PSVT	68	M	0	1767	0.00%	752	71	52	47	174	13.78%	55%
<i>L</i>	LVH/PE	43	M	0	1373	0.00%	873	11	18	78	0	0.00%	77%
<i>M</i>	VHD/LVH	57	M	0	1733	0.00%	692	8	16	78	0	0.00%	74%
<i>N</i>	LVH	32	M	0	1288	0.00%	931	36	49	219	172	13.37%	59%
<i>O</i>	LVH/PE	72	M	0	1735	0.00%	691	11	11	63	1	0.06%	65%
<i>P</i>	VHD	71	F	0	1427	0.00%	840	15	33	141	6	0.42%	79%
Mean		66.19		0.94	1474.38	0.06%	829.00	26.13	28.25	103.56	35.75	2.70%	68.88%
±1 SD		14.49		3.75	182.92	0.23%	90.66	20.61	15.40	49.77	57.24	4.48%	7.21%
AF	Diagnosis	Age	Sex	PVC	TB	PVC/TB	Mean	RMSSD	SDNN	TINN	NN50	PNN50	EF
<i>a</i>	VHD/PH	60	M	1	1321	0.08%	912	231	167	656	849	80.02%	78%
<i>b</i>	LVH	73	M	4	1816	0.22%	664	154	110	484	958	69.42%	73%
<i>c</i>	VHD/PH	89	F	1	1358	0.07%	896	313	225	781	844	84.40%	69%
<i>d</i>	LVH/PAC	62	M	51	1372	3.72%	896	288	174	141	422	70.10%	72%
<i>e</i>	LVH	56	M	0	1592	0.00%	758	349	233	516	950	83.41%	61%
<i>f</i>	PH	82	F	3	1539	0.19%	782	182	129	516	916	75.27%	86%
<i>g</i>	VHD/LVH	68	M	1	1530	0.07%	783	234	169	375	961	76.70%	80%
<i>h</i>	LVH	81	M	2	1727	0.12%	700	183	133	484	995	73.78%	72%
<i>i</i>	VHD/IHD	87	M	0	1217	0.00%	998	280	216	906	689	80.98%	77%
<i>j</i>	VHD/LBBB	80	F	2	990	0.20%	1214	417	304	503	688	85.36%	59%
<i>k</i>	LVH/PAC	54	F	0	1013	0.00%	1190	145	93	266	687	71.34%	79%
<i>l</i>	RHD	57	F	0	1434	0.00%	838	217	166	438	907	75.46%	65%
<i>m</i>	LVH/VHD	79	M	0	1360	0.00%	890	222	172	656	851	78.87%	71%
<i>n</i>	VHD/PH	73	M	21	1097	1.91%	1105	267	202	672	700	81.30%	57%
<i>o</i>	LVH/VHD	68	F	9	1455	0.62%	845	286	161	141	267	45.49%	80%
<i>p</i>	LVH	73	F	0	1200	0.00%	932	341	212	63	521	86.69%	69%
Mean		71.38		5.94	1376.31	0.45%	900.19	256.81	179.13	474.88	762.81	76.16%	71.75%
±1 SD		11.21		13.15	236.90	0.99%	160.41	75.26	52.43	236.07	211.91	9.80%	8.23%

AF = Atrial fibrillation; EF = Ejection fraction; F = Female; IHD = Ischemic heart disease; LBBB = Left bundle branch block; LVH = Left ventricular hypertrophy; M = Male; PH = Pulmonary hypertension; PAC = Premature atrial contraction; PE = Pericardial effusion; PPM = Permanent pacemaker implantation; RBBB = Right bundle branch block; SD = Standard deviation; SR = Sinus rhythm; SVT = Supraventricular tachycardia; VHD = Valvular heart disease.

Table 3. Gross median error for SST-IF in the segments of 5, 10, and 60 seconds (E_5 , E_{10} , and E_{60})

SR	E_5	E_{10}	E_{60}
<i>A</i>	2.21%	1.96%	1.01%
<i>B</i>	0.96%	0.76%	0.26%
<i>C</i>	0.59%	0.63%	0.22%
<i>D</i>	0.63%	0.46%	0.17%
<i>E</i>	0.77%	0.66%	0.32%
<i>F</i>	1.58%	1.49%	0.59%
<i>G</i>	0.36%	0.33%	0.21%
<i>H</i>	1.17%	0.99%	0.30%
<i>I</i>	0.65%	0.53%	0.16%
<i>J</i>	0.49%	0.43%	0.14%
<i>K</i>	0.63%	0.54%	0.21%
<i>L</i>	0.90%	0.73%	0.40%
<i>M</i>	0.41%	0.32%	0.09%
<i>N</i>	1.30%	1.08%	0.44%
<i>O</i>	0.65%	0.51%	0.20%
<i>P</i>	1.05%	0.99%	0.37%
Mean±1SD	0.90±0.48%	0.78±0.44%	0.32±0.22%
AF	E_5	E_{10}	E_{60}
<i>a</i>	1.89%	1.74%	0.93%
<i>b</i>	1.53%	1.29%	0.32%
<i>c</i>	2.11%	1.90%	0.78%
<i>d</i>	2.11%	1.56%	1.24%
<i>e</i>	2.15%	1.87%	0.72%
<i>f</i>	3.32%	2.90%	1.87%
<i>g</i>	1.61%	1.22%	0.34%
<i>h</i>	1.63%	1.42%	0.27%
<i>i</i>	0.77%	0.73%	0.15%
<i>j</i>	3.83%	3.39%	2.41%
<i>k</i>	2.04%	1.94%	3.10%
<i>l</i>	1.00%	0.89%	0.28%
<i>m</i>	1.68%	1.55%	0.59%
<i>n</i>	1.55%	1.39%	0.82%
<i>o</i>	2.43%	1.95%	3.28%
<i>p</i>	1.86%	1.29%	0.79%
Mean±1SD	1.97±0.76%	1.69±0.68%	1.12±1.01%

Table 4. Clinical characteristics, HRV profiles, and cardiac systolic function of selected patients with sleep apnea/Cheyne-Stoke respiration

SR	Diagnosis	Age	Sex	PVC	TB	PVC/TB	Mean	RMSSD	SDNN	TINN	NN50	PNN50	EF
<i>Q</i>	IHD/CVA	58	M	19	1593	1.19%	753	14	18	78	4	0.26%	36%
AF	Diagnosis	Age	Sex	PVC	TB	PVC/TB	Mean	RMSSD	SDNN	TINN	NN50	PNN50	EF
<i>q</i>	VHD/LVH	75	M	1	1265	0.08%	954	199	153	594	707	76.56%	75%
<i>r</i>	VHD/PH	88	F	30	1949	1.54%	639	235	167	156	869	78.57%	36%
<i>s</i>	IHD/LBBB	70	M	3	1695	0.18%	713	181	130	391	923	68.62%	45%

AF = Atrial fibrillation; EF = Ejection fraction; F = Female; IHD = Ischemic heart disease; LBBB = Left bundle branch block; LVH = Left ventricular hypertrophy; M = Male; PH = Pulmonary hypertension; CVA = cerebral vascular accident; SR = Sinus rhythm; VHD = Valvular heart disease.

Table 5. Gross median error for the SST-IF in the segment of 5, 10, and 60 seconds (E_5 , E_{10} , and E_{60}) for selected patients with sleep apnea/Cheyne-Stoke respiration

SR	E_5	E_{10}	E_{60}
Q	6.58%	6.31%	7.18%
AF	E_5	E_{10}	E_{60}
q	4.63%	4.83%	3.61%
r	failure	failure	failure
s	6.62%	6.68%	5.24%

Figures

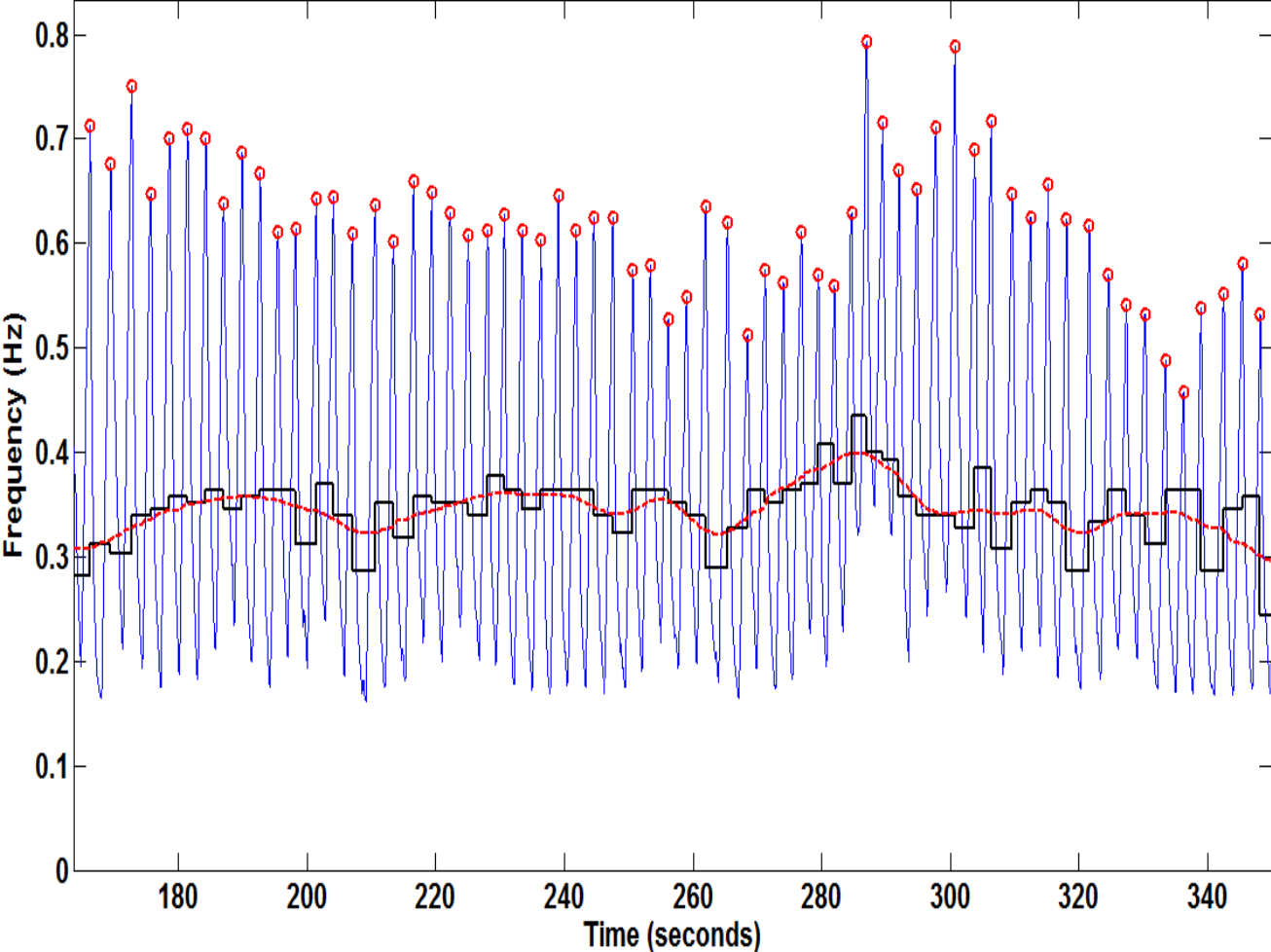


Figure 1

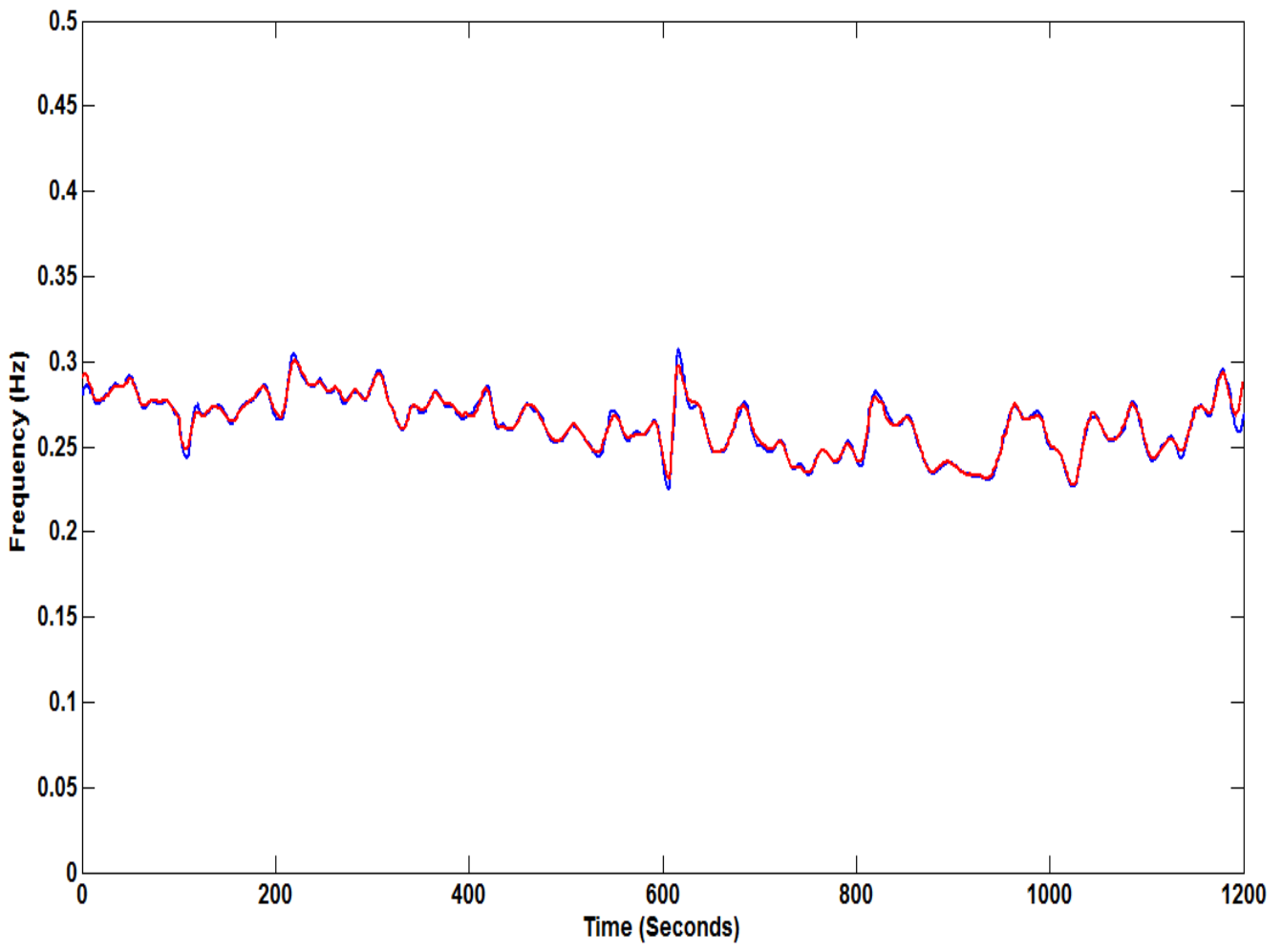


Figure 2

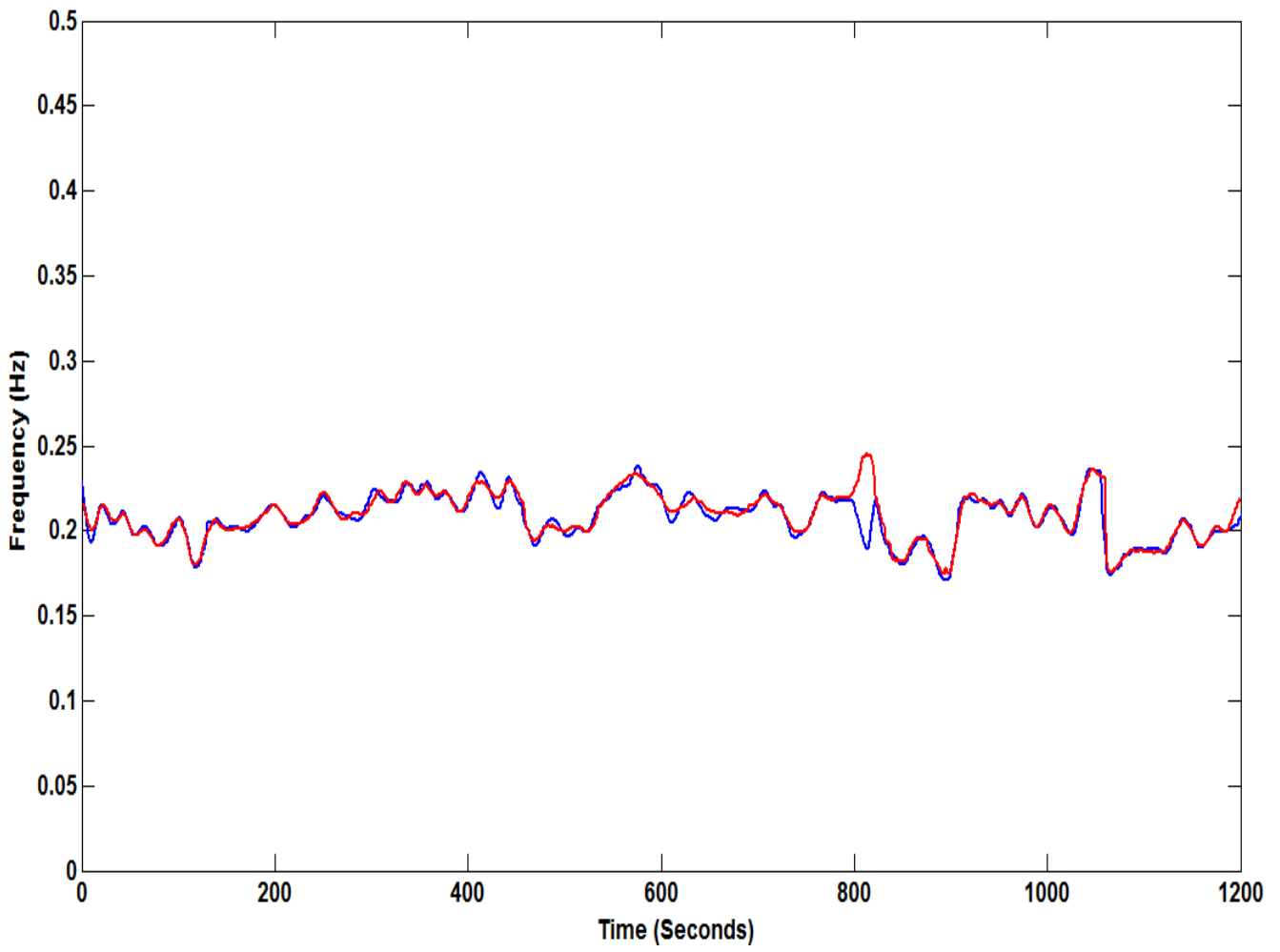


Figure 3

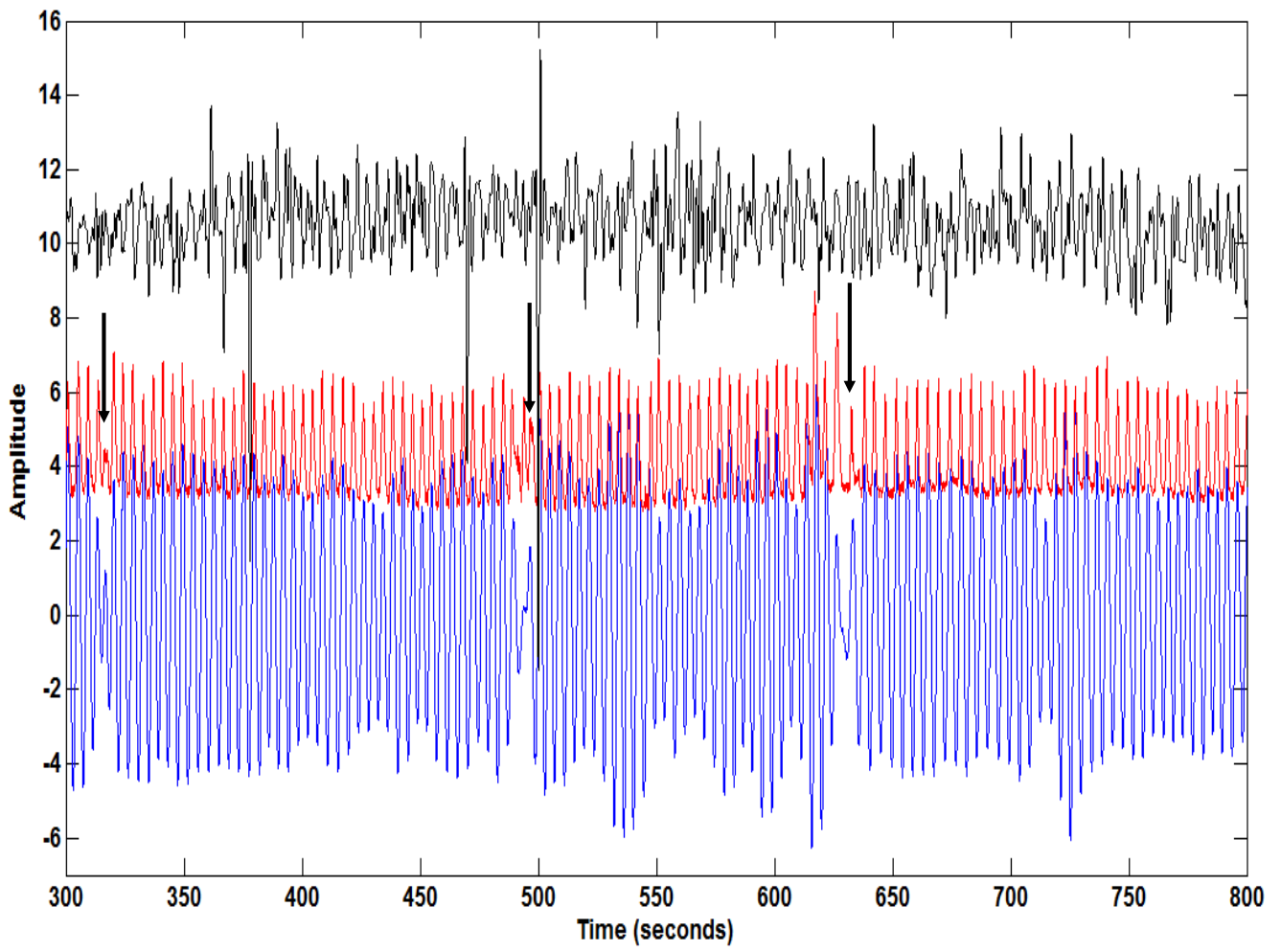


Figure 4

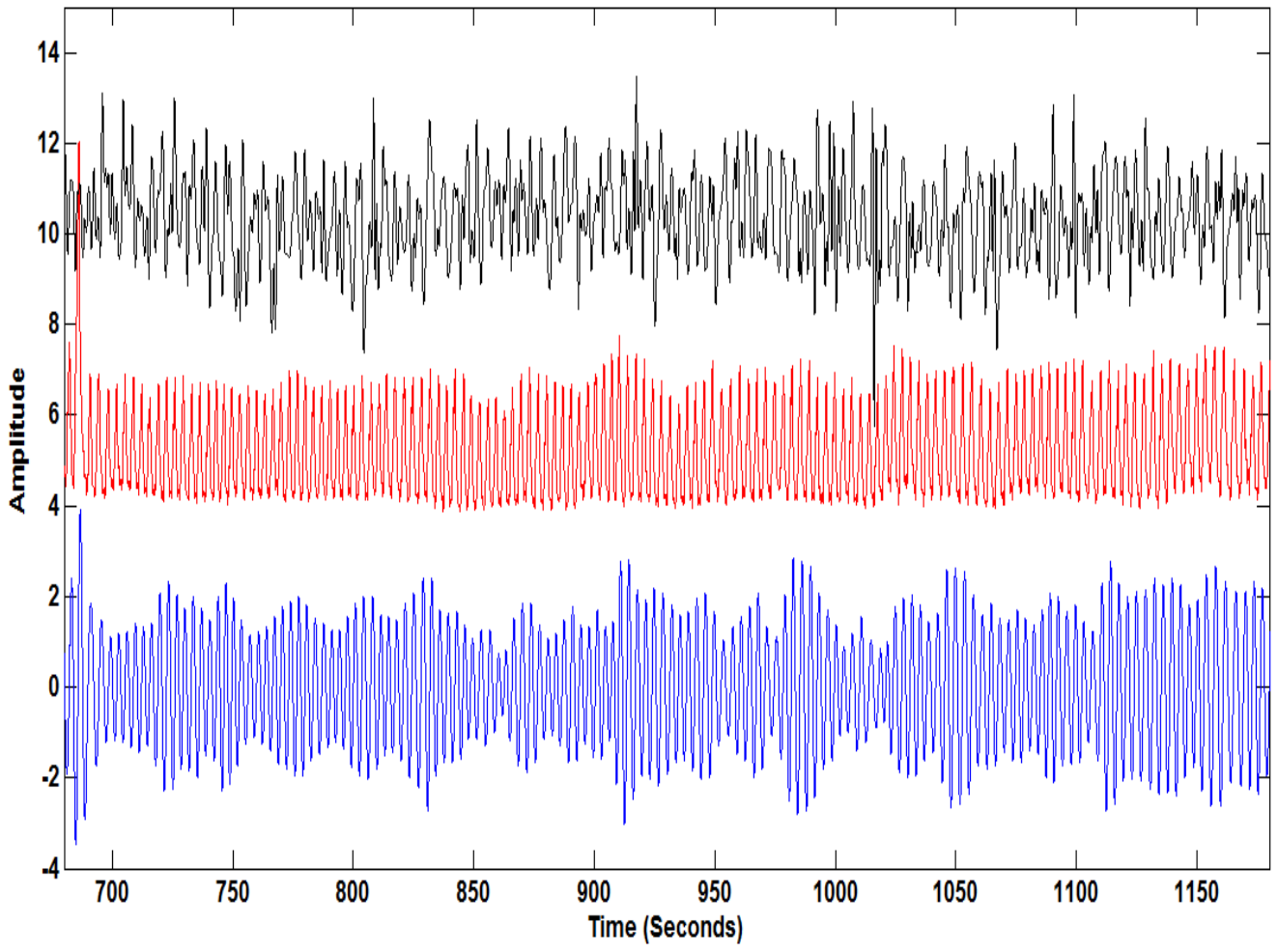


Figure 5

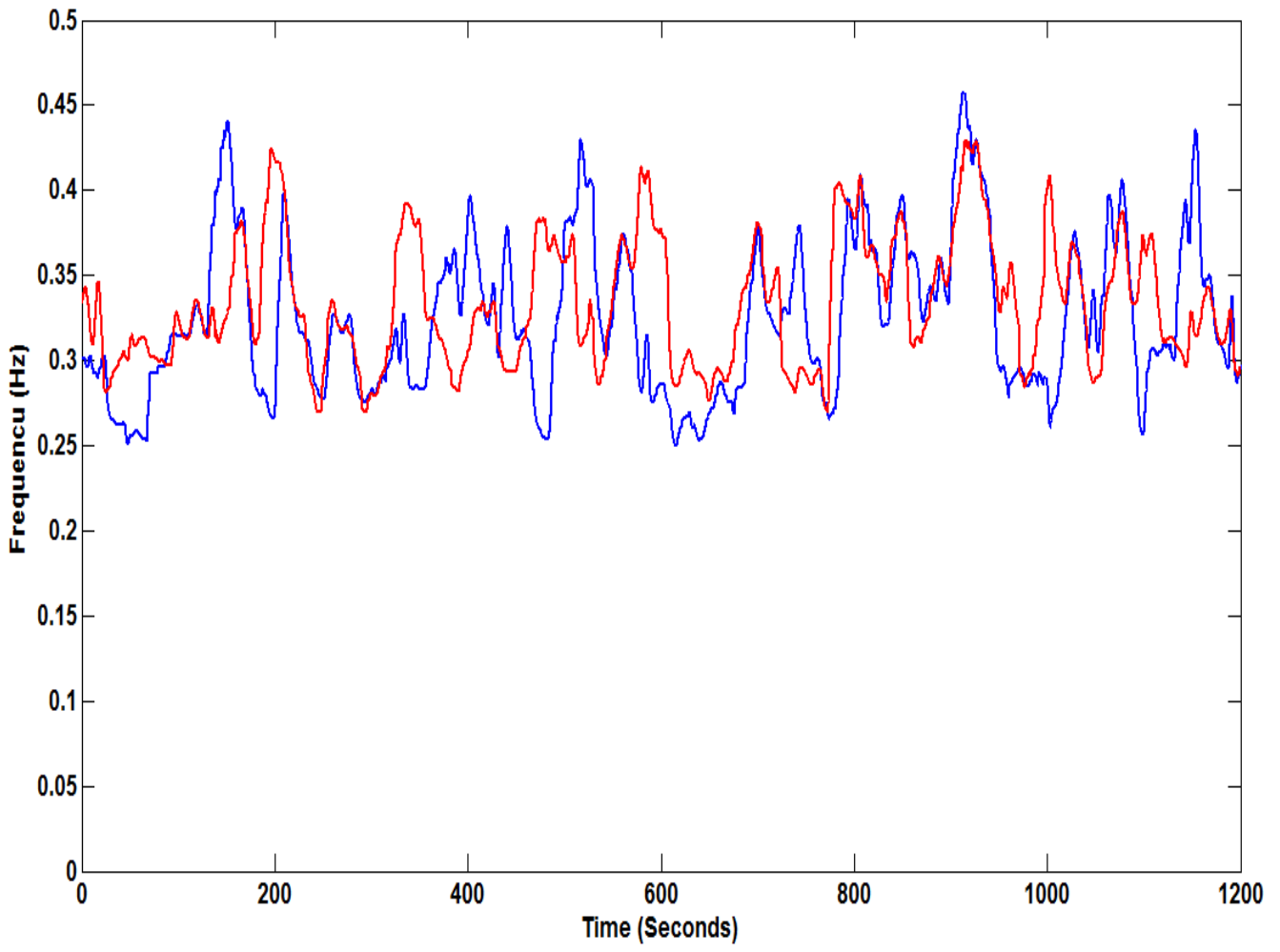


Figure 6

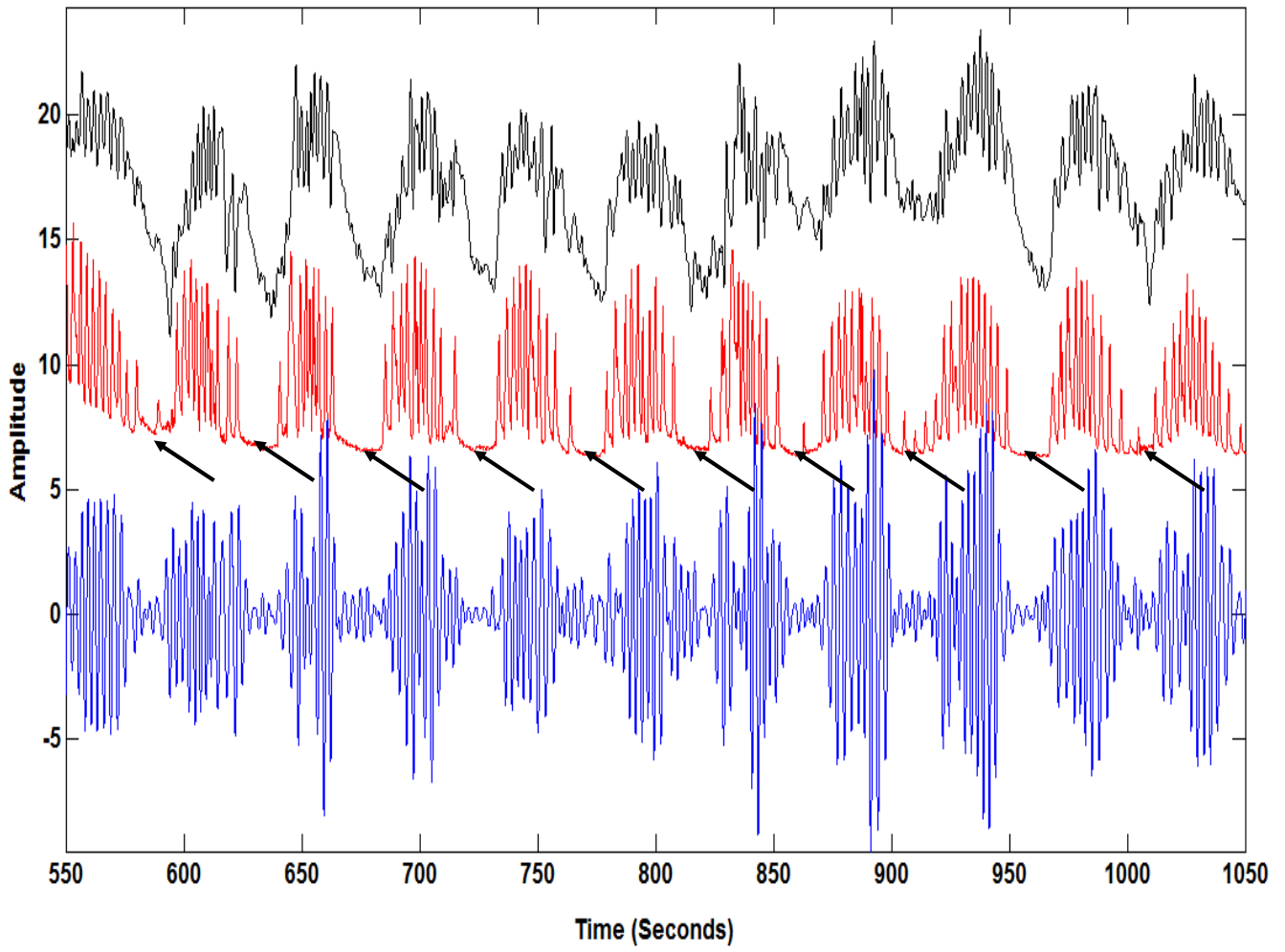
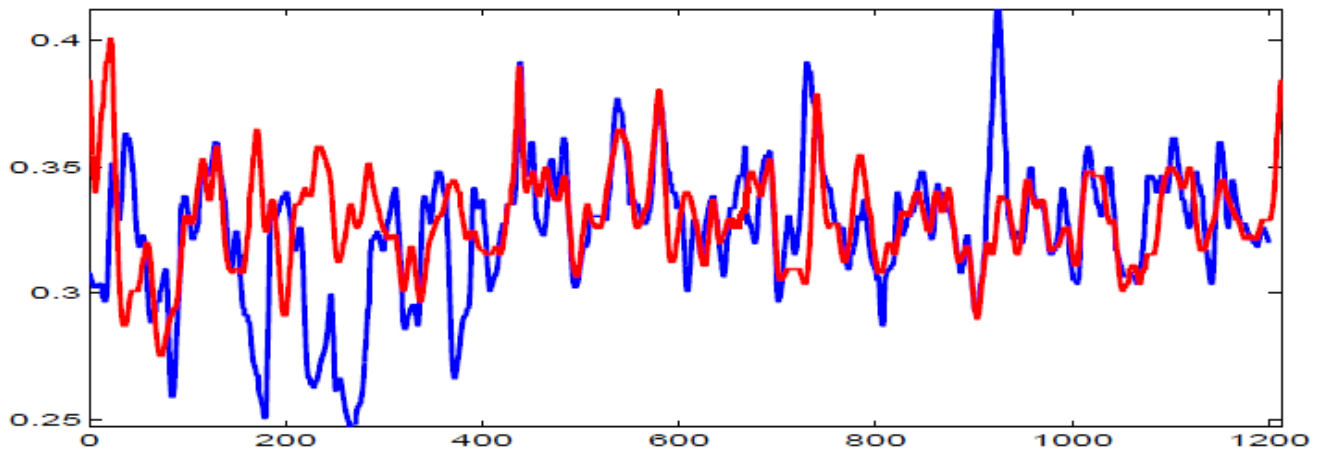


Figure 7

A All PACs are removed



B All PACs are preserved

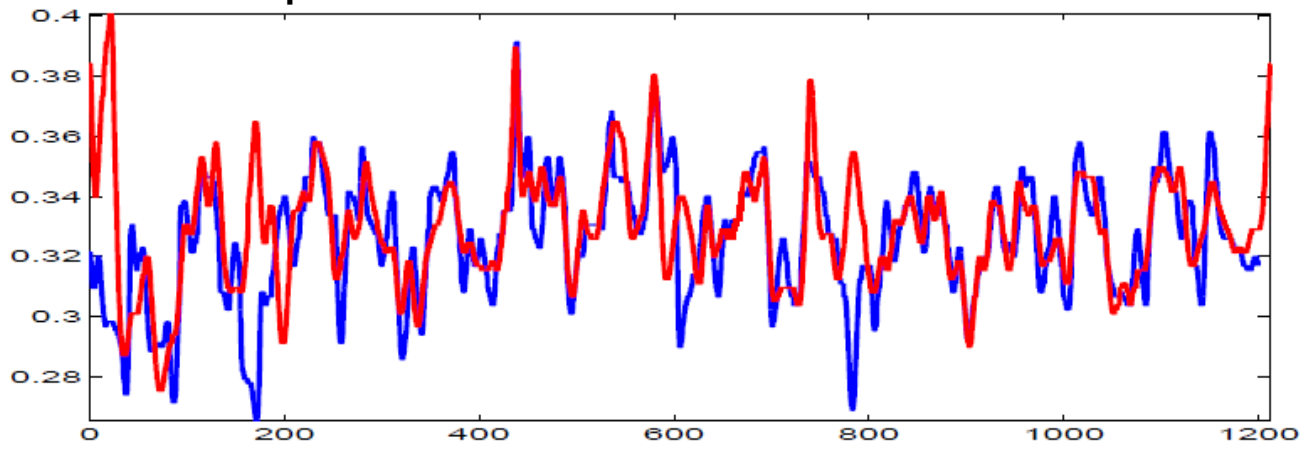
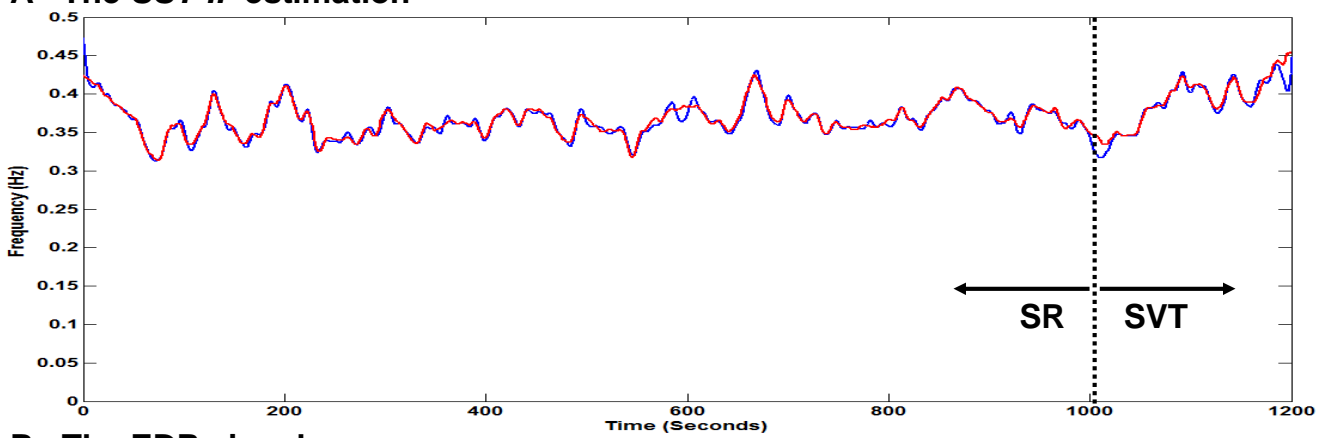


Figure 8

A The SST-IF estimation



B The EDR signal

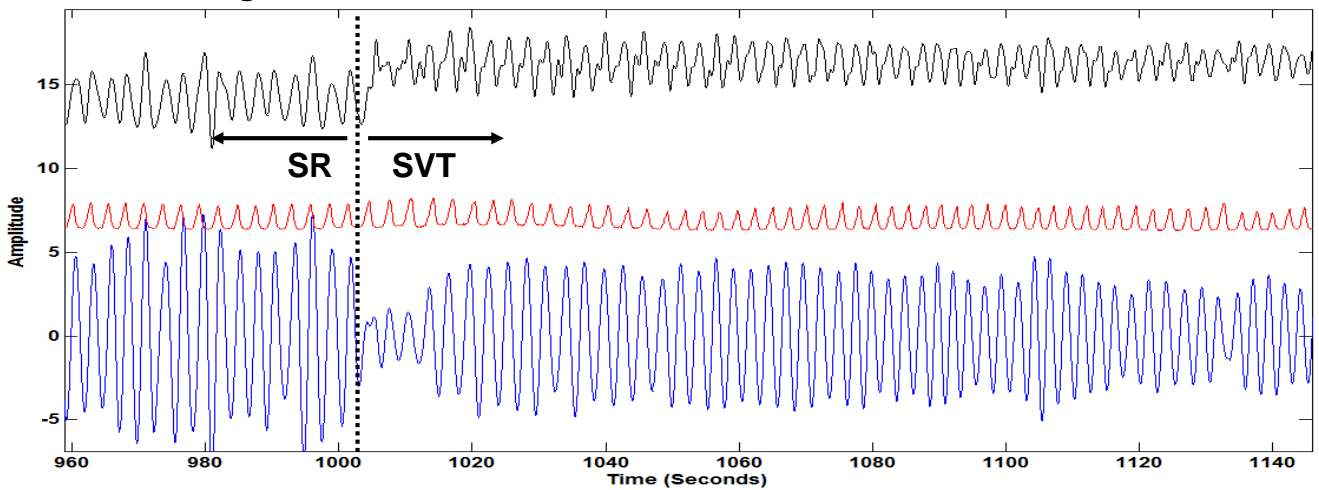


Figure 9